Title	Defect detection using quasi-scholte wave for plate loaded with water on single surface
Author(s)	Hayashi, Takahiro; Fujishima, Rei
Citation	Materials Transactions (2016), 57(9): 1602-1608
Issue Date	2016-01-01
URL	http://hdl.handle.net/2433/217232
Right	©2016 The Japan Institute of Metals and Materials; Publisher permitted posting the final published paper on this repository.
Type	Journal Article
Textversion	publisher

Defect Detection Using Quasi-Scholte Wave for Plate Loaded with Water on Single Surface

Takahiro Hayashi[*] and Rei Fujishima

Graduate School of Engineering, Kyoto University, Kyoto 615–8540, Japan

Ultrasonic guided waves achieve non-destructive inspection of thin plates. However, issues such as large energy leakage and attenuation often plague guided wave inspection of storage tanks and pipes filled with fluid. This study experimentally investigated the non-destructive testing of a water-loaded flat aluminum alloy plate through the application of a quasi-Scholte (QS) wave that propagated along the fluid-plate interface without experiencing attenuation due to leakage. A QS wave was confirmed as having been generated and propagated in a plate loaded with water on the bottom surface using ultrasonic incidence and detection at the top water-free surface. Two-dimensional Fourier transform images of the waveforms revealed reflection of the QS wave from a defect as well as a forward incident QS wave. The visualization results experimentally confirmed—via measurements of waves in water using a laser Doppler vibrometer—that QS waves propagated along a plate surface, while scattered waves were generated by defects.   [doi:10.2320/matertrans.M2016204]

1. Introduction

When an elastic wave with a wavelength greater than the thickness of a plate (or plate-like structure) is incident upon it, elastic wave modes can be observed guiding along the plate. Guided waves propagating in the longitudinal direction with confining elastic wave energy in the cross section are seen to travel farther than bulk waves[1,2]. Guided wave inspection has developed as an efficient inspection technique for elongated structures in the field of non-destructive testing (NDT). For example, Lamb waves have been applied to thin plates, mainly in steel production lines, since the 1950s[1]. In the 1990s, inspection equipment was developed for long-range inspection of pipes[3–8]. In recent times, research has progressed in guided wave inspection for waveguides with complex cross sections such as rails[9–13].

Because guided waves consist of multiple modes with different velocities and dispersions, a single mode with a small dispersion is selectively generated and detected in guided wave inspection. However, in fluid-loaded plate-like structures such as fluid-filled tanks and pipes, energy leakage from the fluid prevents the guided wave mode from propagating long distances. In another paper, the author of this study discussed quasi-Scholte (QS) waves that propagate along fluid-plate interfaces without attenuation due to leakage, using a semi-analytical finite element (SAFE) method for a plate with leaky media[14,15].

Rayleigh waves propagate along the surface of a semi-infinite isotropic homogeneous medium with a traction-free surface, whereas Scholte waves propagate in a semi-infinite isotropic homogeneous medium in contact with a semi-infinite perfect fluid. The guided wave mode travels at the speed of sound in the fluid without radiating energy from the interface between the elastic solid medium and the perfect fluid. It has been theoretically and experimentally proved that the Scholte wave mode does not show a dispersive nature, and that the energy focuses more locally–at the fluid-solid bound-ary–at higher frequencies[1,14–18] like the Rayleigh wave does. When a thin plate contacts with a semi-infinite perfect fluid on a single surface or on both surfaces, a guided wave mode exists at the fluid-plate interface(s), but shows a dispersion caused by the thickness of the plate. Therefore, this mode is called the quasi-Scholte (QS) wave to distinguish it from the Scholte wave.

As shown by a SAFE calculation performed in Refs. 14) and 15), although the fundamental Lamb modes—called A0 and S0—are generally used in NDT for a plate, they cannot travel long distances in a fluid-loaded plate due to large attenuation through energy leakage. Hence, a QS wave has the potential as an alternative mode for long-range guided wave inspection. This study experimentally investigates the applicability of a QS wave for detection of inner defects such as erosion and corrosion in tanks and pipes filled with a fluid.

2. Characteristics of a QS Wave in a Plate Loaded with Water on a Single Surface

A fundamental analysis of tanks and pipes filled with water was conducted on a homogeneous aluminum plate (longitudinal wave velocity: 6400 m/s, transverse wave velocity: 3100 m/s, density: 2.7 kg/m^3, thickness: d) in contact with water (sound wave velocity: 1500 m/s, density: 1.0 kg/m^3) on a single surface. Phase velocity (c) dispersion curves, group velocity (c_g) dispersion curves, and attenuation (α) curves were calculated using a SAFE method[14] as shown in Figs. 1(a), 1(b), and 1(c), respectively. In the figures, solid lines and dashed lines denote the curves for a plate with and without water, respectively, while the horizontal axes show frequency-thickness products fd. In the fd range shown here, A0 and S0 modes with anti-symmetric and symmetric wave distributions exist for a plate without water, while a QS wave (solid black line) appeared for a plate loaded with water on a single surface in addition to A0-like and S0-like modes. The QS wave does not show dispersion in the fd range over 500 kHz mm, while the QS wave has strong dispersion in the fd range below 400 kHz mm. However, because attenuation

*Corresponding author, E-mail: hayashi@kuaero.kyoto-u.ac.jp

(a) Phase velocity

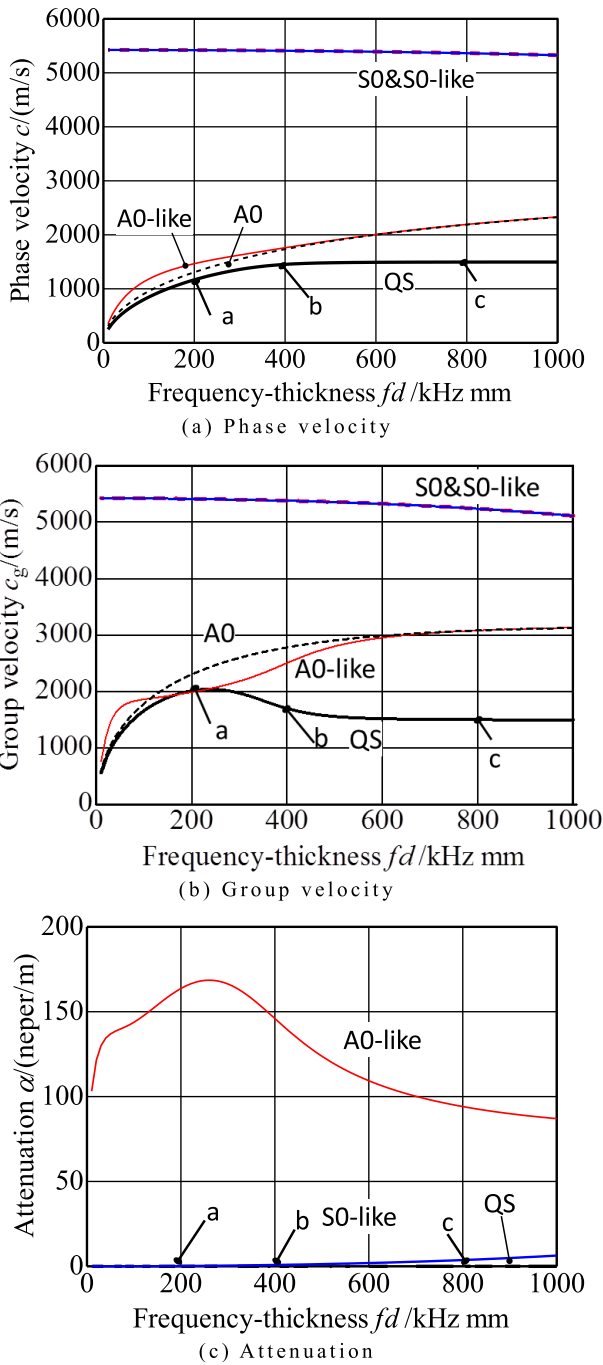(b) Group velocity

(c) Attenuation

Fig. 1   Dispersion curves for an aluminum plate with thickness d. Solid lines: a water-loaded plate on a single surface. Dashed lines: a water-free plate. (a) Phase velocity, (b) Group velocity, (c) Attenuation.

(a) 200 /kHz mm

(b) 400 /kHz mm

(c) 800 /kHz mm

Fig. 2   Displacement distributions for QS waves at three different fd values. (a) 200 kHz mm, (b) 400 kHz mm, (c) 800 kHz mm.

of the QS wave is zero over the entire fd range, the QS wave may have the potential for long-range propagation even in the dispersive low-fd range. The solid red and blue lines are similar to the curves for the A0 and S0 modes (dashed lines) in Fig. 1(a) and 1(b). Because these modes, shown in solid red and blue lines, do not have perfectly anti-symmetric and symmetric distributions with respect to the centerline of the plate loaded with water on a single side, they are called A0-like and S0-like modes in this paper.

Figures 2(a)–(c) show wave structures at a–c in Fig. 1, in the area of $10d \times 6d$ in the propagation and thickness directions respectively. An aluminum alloy plate with thickness d is located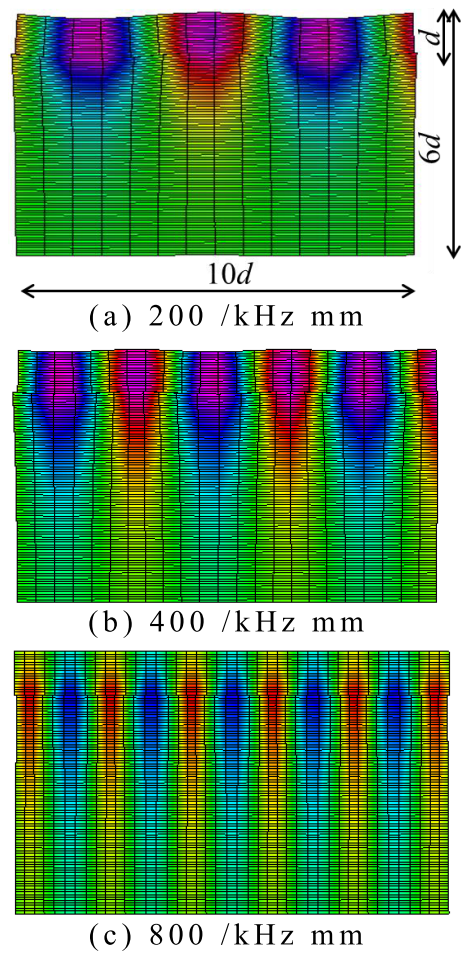 in the upper region, while the lower region has a water area with depth $5d$. The grid motion shows the displacements, and the color denotes the displacement in the direction of thickness. At 200 kHz mm shown in Fig. 2(a), a flexural vibration distributes itself over the whole cross section of the plate, while the vibration is localized in the vicinity of the plate surface in water. At 400 kHz mm shown in Fig. 2(b), a flexural vibration distributes itself over the whole cross section of the plate as it does in (a), and in the water, the vibration distributes itself slightly farther from the plate surface than in (a). The distribution in water is opposed to the tendency of Scholte waves to focus locally at the fluid-solid boundary, at higher frequencies. At 800 kHz mm shown in Fig. 2(c), plate vibration is concentrated on the lower surface. In this fd range, vibration concentrates more at the water-plate boundary in both the plate and water, which is similar to the tendency of Scholte waves in bulky media. In addition, because phase and group velocities are almost constant in the fd range over 800 kHz mm, the interface wave can be regarded as a Scholte wave in the high-frequency range.

A QS wave provides largely different wave structures in frequency as shown in Fig. 2 and Ref. 15). This implies that the detectability of defects in a plate varies with frequency. To show this more clearly, Fig. 3 shows (a) energy flow rate in the plate, and (b) energy density distributions in a cross section for the three fd values. (a) is the flow rate of energy in the plate for the entire transmission energy. Vibration energy
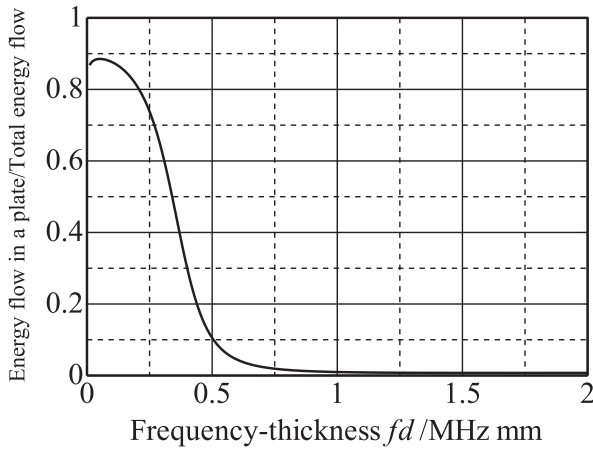
(a) Energy flow rate
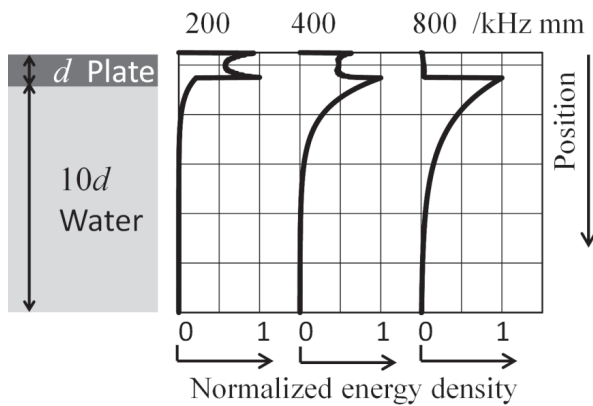
(b) Energy flow distributions

Fig. 3 Energy flow for a QS wave. (a) Energy flow rate, (b) Energy flow distributions.

Fig. 4 Experimental set-up and measurement conditions.

propagates less than 10% of the entire energy in the *fd* range over 500 kHz mm, and the plate energy becomes smaller in a higher *fd* range. This fact implies that waves reflected from defects in a plate become smaller in higher *fd* ranges. On the contrary, more than 80% of the entire energy exists in a plate in the *fd* range below 200 kHz mm, and therefore, this frequency range may be suitable for NDT of a plate from the viewpoint of energy flow. However, because the QS wave has a large dispersion in the low frequency range below 200 kHz mm as shown in Figs. 1(a) and 1(b), it might be difficult to use it for long range NDT. Figure 3(b) shows the energy density distributions in a cross section of the plate and water for the three *fd* values—200 kHz mm, 400 kHz mm, and 800 kHz mm. As described later, it might be more difficult to detect a QS wave at 800 kHz mm and 400 kHz mm than at 200 kHz mm because the energy density becomes much smaller for higher *fd* values at the free surface of a plate, from which the ultrasonic wave is generated and detected.

3. Experiments

3.1 Experimental set-up
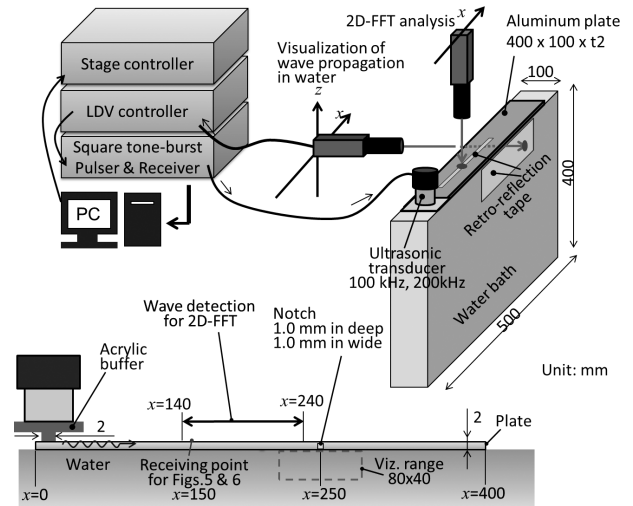
An experimental set-up as shown in Fig. 4 was used to measure QS waves. An aluminum alloy plate of dimensions 400 mm × 100 mm × 2 mm was placed on an acrylic water bath measuring 500 mm × 400 mm × 100 mm, filled with water. An ultrasonic wave was generated at one end of the plate by longitudinal wave transducers with the center frequencies of 100 kHz and 200 kHz. Three-cycle rectangular burst signals of 100 kHz and 200 kHz were input from an ultrasonic pulser receiver (Japan probe, JPR-10B) to the transducers.

Typically, an angle beam wedge is installed between the ultrasonic transducer and plate to generate a single A0 or S0 mode of Lamb waves efficiently. If the longitudinal wave velocity in a wedge is c_W and the phase velocity of the required Lamb wave is c, then θ, the incident angle of the wedge for efficient generation of the mode, can be determined as

$$\sin \theta = c_W / c. \tag{1}$$

However, the phase velocity of a QS wave is lower than the speed of sound in water, as shown in Fig. 1 ($c \leq 1500$ m/s), while the longitudinal velocity of a solid wedge is generally higher that the speed of sound in water ($c_W > 1500$ m/s). It is therefore not possible to find an appropriate incident angle using eq. (1) to generate a QS wave efficiently. Therefore, in this study, an acrylic buffer was installed instead of using a wedge (Fig. 1). The acrylic buffer consists of a line protuberance 2 mm in width that is smaller than half the wavelength of the A0 mode and QS wave at 100 kHz and 200 kHz. Bringing the line protuberance in contact to one edge of the plate (letting the plate edge be $x = 0$), it works as a line source to generate guided waves in the $\pm x$ directions. The waves reflected backwards from the edge of the plate, and the forward waves, are both superposed when the line source is located at an appropriate position. In all the experiments, the position of the line source was precisely adjusted for achieving the largest signals.

First, vibrations in the direction of thickness were detected on the upper surface of the plate using a laser Doppler vibrometer (LDV, Onosokki LV-1710). A retro-reflection tape was attached to the measurement area for ensuring stable laser measurements, which enabled the measurement of out-of-plane vibrations with linear automatic stages at many points from $x = 140$ mm to 240 mm in the next section. The dilata-
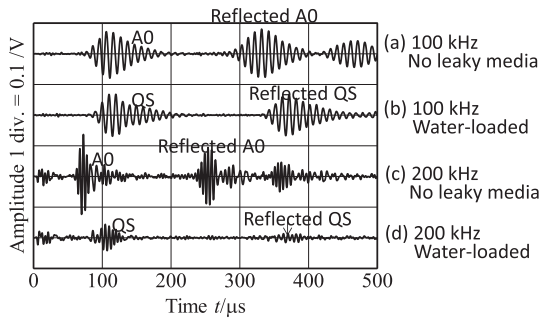
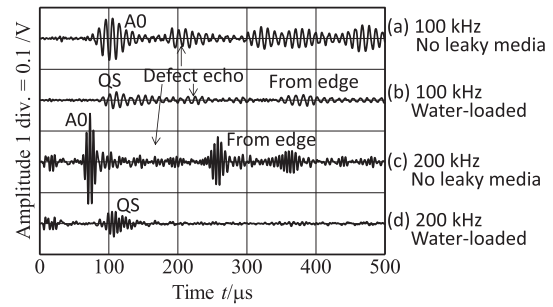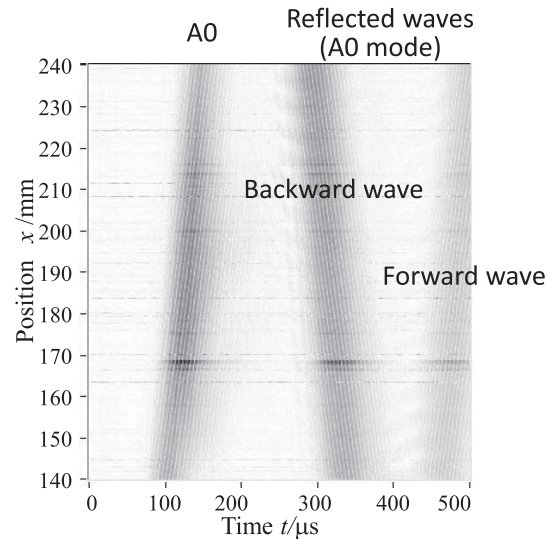Fig. 5   Waveforms for an defect-free plate.

Fig. 6   Waveforms for a plate with a defect.

Fig. 7   *t-x* image for a water-free and defect-free plate.

tional wave was detected in water using laser emission from the transparent side wall of the water bath and the reception of the reflected beam from the opposing side wall on which a retro-reflection tape was attached. The laser measurements utilized the small changes in refractive index that occurred because of waves in water[19,20]. Animations of wave propagation in water were created using multiple waveforms measured in the area of 80 mm × 40 mm in Fig. 4.

3.2 Modal analysis using two-dimensional Fourier transform

This section discusses a QS wave through the measurements at the upper surface of the plate. Figure 5 shows the waveforms for the plate without a defect, measured at $x = 150$ mm: Fig. 5(a) 100 kHz incidence and a water-free plate, Fig. 5(b) 100 kHz incidence and a water-loaded plate, Fig. 5(c) 200 kHz incidence and a water-free plate, and Fig. 5(d) 200 kHz incidence and a water-loaded plate.

In Fig. 5(a), the first wave packet arriving between 80 μs and 200 μs is determined to be an A0 mode that traveled about 150 mm from the line source by the group velocity dispersion curves for a water-free plate (the dashed lines in Fig. 1(b)). The second and third wave packets in Fig. 5(a) are the A0 mode reflected at the right and left edges of the plate. In Fig. 5(b), the wave packets appear slightly later than the ones in Fig. 5(a). Because a QS wave and an A0-like mode for a water-loaded plate have slightly smaller group velocities at 100 kHz than the one with the A0 mode for a water-free plate as shown in Fig. 1(b), the wave packets in Fig. 5(b) may be a QS wave and an A0-like mode. Considering that an A0-like mode in a water-loaded plate can have a large attenuation as shown in Fig. 1(c), the wave packets in Fig. 5(b) can be estimated to be the QS wave. This is revealed more clearly using a two-dimensional Fourier transform analysis later in the paper. In Fig. 5(c) and Fig. 5(d) for a 200 kHz incidence, electromagnetic noises appeared from a time of 0 μs to 50 μs because high voltage signals were required by the ultrasonic transducer. Thereafter, in Fig. 5(c) for a water-free plate, the first wave packet was observed between 50 μs and 150 μs, and the second and third ones appeared at approximately 250 μs and 350 μs, respectively. From the group velocity dispersion curves (the dashed lines in Fig. 1(b)), these wave packets are apparently the incident and reflected waves of the A0 mode. In Fig. 5(d) for a water-loaded plate, the first and second wave packets appeared at approximately 100 μs and 350 μs, slightly later than the ones in Fig. 5(c), which indicates that these are QS waves that have a smaller group veloc-

ity than the A0 mode for a water-free plate at 200 kHz, as shown in Fig. 1(b).

Figure 6 shows waveforms that were recorded for a plate with an artificial rectangular notch 1.0 mm in width and 1.0 mm in depth engraved on the back surface at $x = 250$ mm, using the same conditions as Fig. 5. Because the first wave packets appeared at the same moment as Fig. 5, they can be estimated to be an A0 mode for a water-free plate and a QS wave for a water-loaded plate. Between the first and second wave packets at 100 kHz, small waves appeared unlike anything in Fig. 5. These waves are reflected waves from the defect. On the other hand, at 200 kHz, reflected waves were not detected clearly owing to small signal-to-noise ratio (SNR).

In Figs. 5 and 6, the detected modes were estimated for a single waveform from the arrival time and theoretical group velocity dispersion curves. However, the guided wave modes were not identified for the first wave packet in Fig. 5(b) and the reflected waves in Fig. 6. Therefore, in this section, dispersion curves are experimentally obtained using a two-dimensional Fourier transform of multiple waveforms detected on the plate surface.

Figure 7 is a time (t)-position (x) image showing absolute values of time-domain waveforms at 401 different positions, at regular intervals in the x direction for a water-free defect-free plate. The receiving positions were 401 points from $x = 140$ mm to $x = 240$ mm at intervals of 0.25 mm on the centerline of the plate width, as shown in Fig. 4. The input
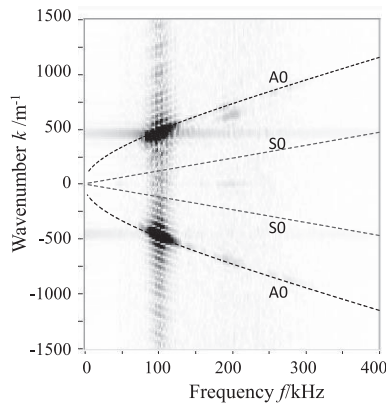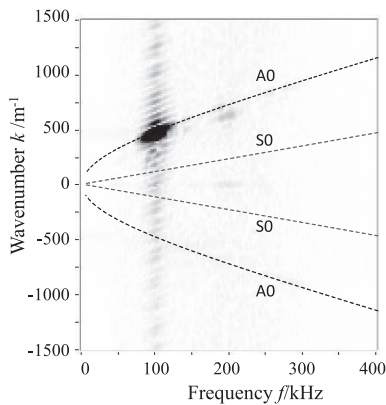
(a) Whole waveforms

(b) Extracted waveforms from 0 µs to 250 µs

Fig. 8 f-k images for a water-fee and defect-free plate. (a) Whole waveforms (b) Extracted waveforms from 0 to 250 µs.
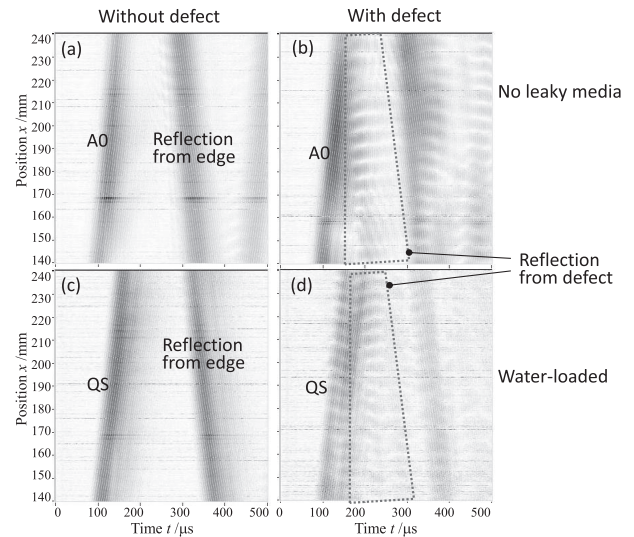

Fig. 9 t-x images for an incidence of 100 kHz. (a) A water-free intact plate (b) A water-free plate with defect (c) A water-loaded intact plate (d) A water-loaded plate with defect.

signal to the ultrasonic transducer was 3-cycle rectangular burst waves at 100 kHz. The waveform in Fig. 5(a) corresponds to the data at $x = 150$ mm in Fig. 7. Three dark bands can be clearly seen in the t-x image. Since the slopes of the dark bands correspond to the group velocities of the propagating waves, the dark bands indicate—from the left to the right—an incident A0 mode propagating in the $+x$ direction, a reflected A0 mode in the $-x$ direction, and a reflected A0 mode in the $+x$ direction.

Calculating Fourier transforms of the 401 waveforms in the time and space directions provided a two-dimensional Fourier transform image in a frequency (f) and wavenumber (k) domain as shown in Fig. 8(a). The dashed lines denote theoretical dispersion curves calculated with the SAFE method for a 2 mm aluminum alloy plate. The data in the x direction is converted to the k direction, and hence $\pm k$ domains indicate guided waves propagating in the $\pm x$ directions. Because the measured data shown in Fig. 7 contain both forward and backward waves, dark areas are located in both $\pm k$ domains, as shown in Fig. 8(a). The dark areas are located on the theoretical dispersion curve of the A0 mode, which proves that the detected waveforms were the A0 modes. Fig. 8(b) shows an f-k image converted using the extracted waveforms between 0 µs and 250 µs that contain only an incident A0 mode traveling in the x direction. The dark area is located on the A0 curve only in the $+k$ domain in Fig. 8(b) as expected.

To compare the results for 100 kHz incidence, Fig. 9 shows t-x images for (a) a water-free and defect-free plate, (b) a water-free plate with defect, (c) a water-loaded intact plate, and (d) a water-loaded plate with defect, where Fig. 9(a) is the same figure as Fig. 7. Comparing Fig. 9(a) and Fig. 9(c), which show the differences between water-free and water-loaded plates, the dark bands for forward and backward waves can typically be seen, but the slopes of the bands are slightly different. This agrees well with theoretical prediction for group velocity dispersion curves (Fig. 4(b)) that a QS wave is slightly slower than an A0 mode for a water-free plate at 200 kHz mm (= 100 kHz × 2 mm). Next, comparing Fig. 9(a) and Fig. 9(b) for differences by defect, it can be found in the t-x image that waveforms after the first wave packet are distorted in Fig. 9(b). Similar distortions in waveforms can be seen in Fig. 9(d). The wave distortions after the first dark band were apparently caused by reflections from the defect.

Figure 10 shows f-k images using extracted waveforms between 0 µs and 250 µs as done in Fig. 8(b). The waveforms contain an incident wave from the line source and a reflected wave from the defect, but no reflected wave from the edge of the plate at $x = 400$ mm. Figures 10(a)–(d) correspond to Fig. 9(a)–(d), respectively. For an defect-free plate (Fig. 10(a) and Fig. 10(c)), dark areas cannot be seen in the $-k$ domain, which indicates that there is no reflection, while dark areas are located in the $-k$ domain in Fig. 10(b) and Fig. 10(d) for a defected plate, which shows reflection from the defect. It can also be found from the theoretical dispersion curves that the reflected waves from the defect were an A0 mode for the water-free plate and a QS wave for the water-loaded plate.

Figures 11 and 12 show t-x images and f-k images for an incidence of 200 kHz. The slopes of dark bands in Fig. 11(a) and Fig. 11(c) represent the group velocities at 400 kHz mm (= 200 kHz × 2 mm), and these modes are identified from Fig. 1(b) as an A0 mode and a QS wave, respectively. For a plate with defect (Fig. 11(b)), wave distortions were seen unlike in Fig. 11(a), which implies the detected waveforms were
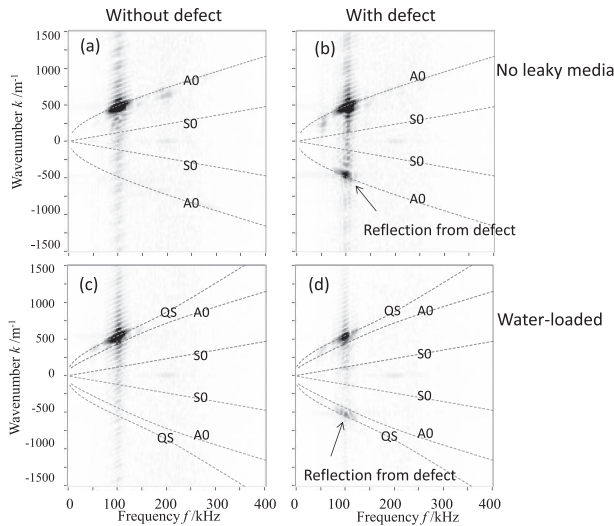
Fig. 10 *f-k* images for an incidence of 100 kHz. (a) A water-free intact plate (b) A water-free defected plate (c) A water-loaded intact plate (d) A water-loaded defected plate.
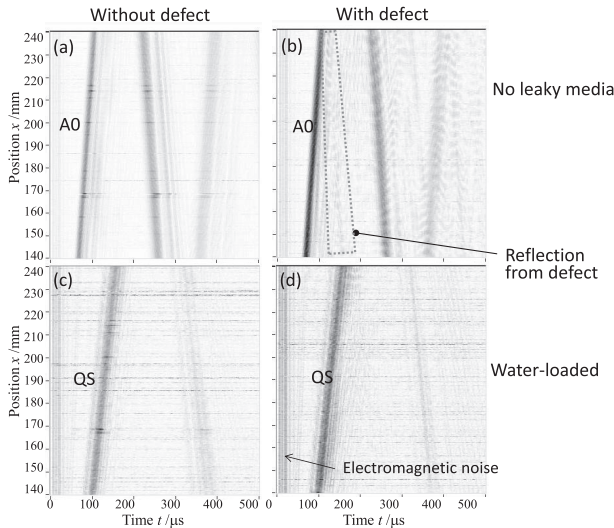

Fig. 12 *f-k* images for an incidence of 200 kHz. (a) A water-free and defect-free plate (b) A water-free plate with a defect (c) A water-loaded and defect-free plate (d) A water-loaded plate with a defect.

Fig. 11 *t-x* images for an incidence of 200 kHz. (a) A water-free and defect-free plate (b) A water-free plate with a defect (c) A water-loaded and defect-free plate (d) a water-loaded plate with a defect.

affected by the reflection from the defect. On the other hand, in Fig. 11(d), such wave distortions cannot be seen, owing to a small SNR. Figure 12 shows *f-k* images obtained from the extracted waveforms between 0 µs and 200 µs that may contain an incident wave and a reflected wave from the defect. In Fig. 12(a) and Fig. 12(c), for defect-free plates, dark bands appear only on the theoretical lines of incident A0 and QS, while a small dark band was seen in the $-k$ domain on the A0 mode line in Fig. 12(b). In Fig. 12(d), dark areas cannot be seen well in the $-k$ domain because the reflected QS wave may be too small. This causes the small energy distribution appearing on the upper surface of a plate at higher frequencies as discussed in section 2. These results imply that the frequency band around 100 kHz is more effective for NDT of a 2-mm aluminum alloy plate, than a 200 kHz band. The horizontal dark bands at $k = 0$ denote the unchanged phase in
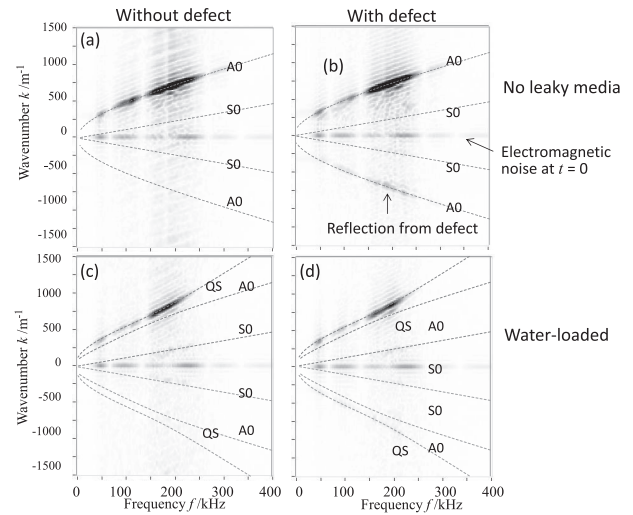
time domain, which is the electromagnetic noise seen around $t = 0$ in Fig. 11.

The aforementioned experimental results prove that normal vibration applied on the surface of a plate predominantly generates an A0 mode in a water-free plate and a QS wave in a water-loaded plate. Similar to the A0 mode of Lamb waves in a plate with a defect, a QS wave can reflect at a defect, and the reflected QS wave can be detected. However, because energy distributions of a QS wave significantly vary in frequency, the appropriate frequency should be selected. In this case, 100 kHz was found to be optimal.

Although a single line source was applied for fundamental experiments in this study, a QS wave can be enhanced with alternative ways. For example, multiple line sources with appropriate delays generate larger a QS wave and a reflected QS wave is enhanced using multiple line receivers by summation of multiple waveforms with appropriate time delays. Using such designated array transducers, a pulse echo inspection may be feasible with the less-dispersive and non-attenuated QS wave.

3.3 Visualization of QS wave in water

In the previous section, QS waves were analyzed by the waveforms detected on the surface of a plate. Since variations in refraction index along the path of a beam can also be measured using LDV, ultrasonic waves can be measured in water by detecting a laser beam passing through it. Measurements of multiple waveforms in water provide an animation of wave propagation in water. In this section, QS waves in water and scattered waves around a defect are visualized by LDV measurements.

A laser beam is rastered over the measurement region of 80 mm × 40 mm in 1.0 mm increments as shown in Fig. 4. Figure 13 is the snapshot of wave distribution at two time steps for an incidence of 100 kHz. The waveforms are normalized by the maximum values of whole signals measured, and the signal values are shown in a color scale, where red and blue indicate 0.2 and −0.2 respectively, while black and white indicate values over ±0.2. In Fig. 13(a) at 590 µs, a QS
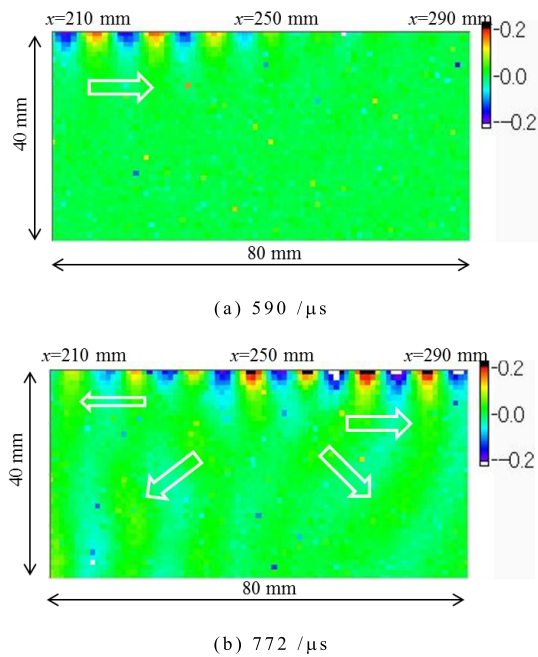
(a) 590 /μs

(b) 772 /μs

Fig. 13 Snapshots of wave propagation in water around a defect for an incidence of 100 kHz. (a) 590 μs (b) 772 μs.
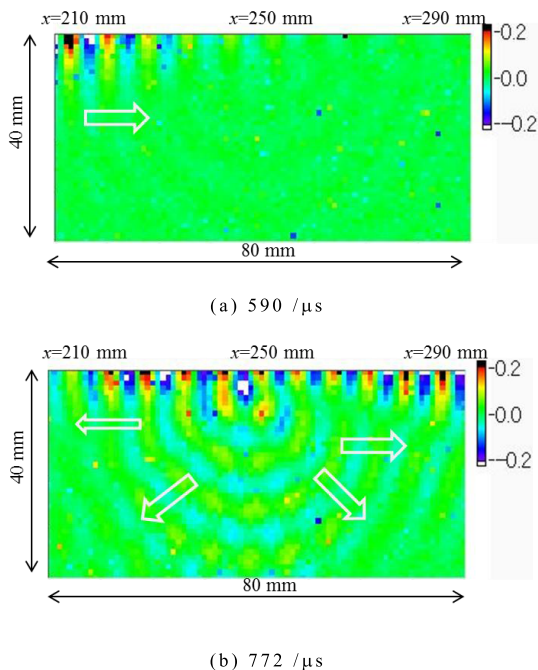

(a) 590 /μs

(b) 772 /μs

Fig. 14 Snapshots of wave propagation in water around a defect for an incidence of 200 kHz. (a) 590 μs (b) 772 μs.

wave propagates from the left to the right along the plate interface. In Fig. 13(b), at 772 μs, when most of the incident QS wave has propagated through the defect, small concentric waves generated at the defect were visualized.

For an incidence of 200 kHz, the snapshots in the same region at the same time steps are shown in Fig. 14. A QS wave with shorter wavelength propagates to the right, and scattered waves radiate at the defect. Although reflected QS waves cannot be ascertained clearly from measurements of the upper surface shown in the previous section, in reality, the incident QS wave reacts significantly at the defect. Low vibration energy is what prevents QS waves from being detected in this frequency range.

4. Conclusions

This paper discussed the guided wave modes that are generated in a plate loaded with water on a single side and reflecting from an inner defect, for use in the NDT of tanks and pipes filled with water. As predicted from group velocity dispersion and attenuation curves, A0 mode and QS wave generation was experimentally confirmed for a water-free plate and a water-loaded plate, respectively. QS waves reflected by a defect were also observed in the two-dimensional Fourier transform images in the frequency–wave number domain. Measurements of multiple waves in water using LDV enabled the creation of QS wave animation in water, and the visualization results revealed that QS waves propagated in water along the plate interface and radiated at the defect. In measurements with a 2 mm aluminum alloy plate, waves reflected from a defect can be obtained at 100 kHz, but not at 200 kHz. This is caused by a QS wave characteristic—the variation of vibration energy distribution in a cross section with frequency. In other words, the choice of an appropriate frequency is essential for conducting NDT using a QS wave.

REFERENCES

1) I. A. Viktorov: *Rayleigh and Lamb Waves*, (Plenum press, New York, 1967).
2) J. L. Rose: *Ultrasonic Waves in Solid Media*, (Cambridge University Press, 1999).
3) D.N. Alleyne, B. Pavlakovic, M.J.S. Lowe and P. Cawley: Insight **43** (2001) 93–96, 101.
4) P.J. Mudge: Insight **43** (2001) 74–77.
5) P. Cawley, M.J.S. Lowe, D.N. Alleyne, B. Pavlakovic and P. Wilcox: Mater. Eval. **61** (2003) 66–74.
6) J.L. Rose: J. Press. Vessel Technol. **124** (2002) 273–282.
7) T. Hayashi and M. Murase: J. Acoust. Soc. Am. **117** (2005) 2134–2140.
8) T. Hayashi and M. Nagao: M. Murase, J. Solid Mech. Mater. Eng. **2** (2008) 888–899.
9) T. Hayashi, W.-J. Song and J.L. Rose: Ultrasonics **41** (2003) 175–183.
10) T. Hayashi, C. Tamayama and M. Murase: Ultrasonics **44** (2006) 17–24.
11) T. Hayashi, M. Murase and T. Abe: Review of Progress in Quantitative Nondestructive Evaluation **26** (2007) 169–176.
12) P.W. Loveday: J. Nondestruct. Eval. **31** (2012) 303–309.
13) S. Mariani, T. Nguyen, R.R. Phillips, P. Kijanka, F. Lanza di Scalea, W.J. Staszewski, M. Fateh and G. Carr: Struct. Health Monit. **12** (2013) 539–548.
14) T. Hayashi and D. Inoue: Ultrasonics **54** (2014) 1460–1469.
15) D. Inoue and T. Hayashi: Ultrasonics **62** (2015) 80–88.
16) S.I. Rokhlin, D.E. Chimenti and A.H. Nayfeh: J. Acoust. Soc. Am. **85** (1989) 1074–1080.
17) D.E. Chimenti and S.I. Rokhlin: J. Acoust. Soc. Am. **88** (1990) 1603–1611.
18) V. Dayal and K. Vikram K: J. Acoust. Soc. Am. **85** (1989) 2268–2276.
19) K. Nakamura: Technical report of IEICE, US2001-9 (2001) pp.15–20 (in Japanese).
20) I. Solodov, D. Döring and G. Busse: Appl. Opt. **48** (2009) C33–C37.